Multi-Objective Optimization Design and Analysis of Double-Layer Winding Halbach Fault-Tolerant Motor

SHUANGSHUANG ZHANG[ID], **WEI ZHANG**[ID], **(Member, IEEE), JIANWEI ZHAO**[ID], **AND RUI WANG**[ID]

School of Electrical Engineering, Nantong University, Nantong 226019, China

Corresponding author: Wei Zhang (zhang.w@ntu.edu.cn)

ABSTRACT Double-layer winding halbach fault-tolerant motor (DLW-HFTM) combines the advantages of the permanent magnet motor and the fault-tolerant motor, which are beneficial to improve the characteristics of the joint robot. First, the structure of DLW-HFTM is proposed in view of the requirement of the fault tolerance of drive motor on the joint robot without degrading the other performances, such as the torque and the efficiency. Then, the working principle and initial design dimensions are depicted, and a finite element parameter model is established by Maxwell software. Furthermore, the design parameters are optimized by multi-objective sensitivity analysis. Finally, the electromagnetic performances before and after optimization are analyzed, including no-load back EMF, torque, loss, efficiency, etc. Meanwhile, the fault-tolerant performance of the motor is analyzed. The research results show that the DLW-HFTM can improve the fault-tolerance on the condition of meeting the design requirements.

INDEX TERMS Robot joints, double-layer winding, halbach fault-tolerant motor, multi-objective optimization, fault-tolerance, quasi-Newton method.

NOMENCLATURE

D_{si}, D_{so}	Inner and outer diameter of stator.
D_{ri}, D_{ro}	Inner and outer diameter of rotor.
H, h_r	Height of stator and rotor.
h_{pm}	Height of permanent magnet.
h_{d1}	Height of stator yoke.
W_{PA}	width of permanent magnet A.
W_{PB}	Width of permanent magnet B_1, B_2.
W_{PC}	Width of permanent magnet C_1, C_2.
α	Magnetizing angle of permanent magnet A.
β_1, β_2	Magnetizing angle of permanent magnet B_1, B_2.
γ_1, γ_2	Magnetizing angle of permanent magnet C_1, C_2.
h_{d2}	height of the upper slot of stator.
h_{d3}	height of the slot wedge of stator.
h_{d4}	height of the lower slot of stator.
W_{d1}	Width of the top of the stator upper slot.
W_{d2}	Width of the bottom of the stator upper slot.
W_{d3}	Width of the top of the lower slot of the stator.
W_{d4}	Width of the stator slot.
d	Radius of the stator opening slot chamfer.
r	Radius of the lower slot of the stator.

The associate editor coordinating the review of this manuscript and approving it for publication was Shihong Ding[ID].

I. INTRODUCTION

Joint robots have the advantages of high stability, high efficiency and high precision. Therefore, it is widely used in bioengineering, medical services, disaster relief, education entertainment and other fields [1], [2]. The drive motor is as the critical element of the joint robot, on which the requirements are getting higher and higher. Thus, it is a research hotspot to develop the joint motor with high efficiency, large torque and low torque ripple.

The main joint motors currently used in robots include stepping motor, direct current motor, and permanent magnet motor [3]–[6]. Among them, permanent magnet synchronous motor (PMSM) has been widely used because of the advantages of small size, large torque and high efficiency. In order

to achieve the design requirements of high efficiency, lager torque, and low torque ripple of joint motors, the structure of PMSM has been further studied to improve the electromagnetic performance [7]–[11]. The spoke-type, tangential-type, U-shape and V-shape permanent magnet structures were compared in [7]. It was found that the PMSM with V-shape permanent magnets could get more comprehensive satisfying results. In [8], halbach PMSM could enhance torque and reduce loss because of the focused magnetic characteristic of Halbach array. In [9], the axial length of PMSM was optimized in order to reduce the loss, improve the efficiency and enhance heat dissipation effect. It was shown in [10] the fundamental wave amplitude of the air-gap magnetic flux density decreased with the increase of the opening width of the semi-closed slot, while the copper loss was increased to maintain the fixed output torque. The torque density of PMSM and fault tolerance could be increased by multi-phase structure [11], [12]. However, the control algorithm, inverter main circuit, and control circuit were more complex, and meanwhile the overall cost was higher than three-phase PMSM. In this paper, a double-layer winding halbach fault-tolerant motor (DLW-HFTM) with special stator structure is proposed, which can be used in various robots, such as industrial robots, agricultural robots and medical robots. It not only has the advantages of high efficiency, large torque and low torque fluctuation, but also has strong fault tolerance. In [13], the magnetomotive force method was used to achieve fault tolerant and minimum loss control of double-star synchronous machines. This method was essentially a current tracking strategy because it did not establish a dynamic model of the motor in phase-deficient operation, and the dynamic performance of the system was reduced because of the pursuit of the steady-state performance of the system. In order to improve the dynamic performance of fault tolerant operation of motor, the accurate dynamic mathematical model was established to complete the decoupled control [14], [15]. Compared with the fault tolerant method with magnetomotive force method, the system complexity of fault tolerant control based on accurate dynamic mathematical model was greatly improved. Therefore, it is very meaningful to improve the fault tolerant performance from the structure of motor, because it is beneficial to simple the control algorithm and reduce the difficulty of fault tolerant control system.

In the process of designing a motor, finite element calculation requires a lot of time and resources. Design time can be greatly reduced by using the intelligent algorithms. Many scholars have introduced various intelligent algorithms into the optimization design of the motor body for different optimization goals [16]–[19]. An ant colony algorithm with continuous domains was used in [20] and the maximal output torque was obtained, but the parameter settings in the algorithm were usually determined by experimental methods, and there were empirical errors. In [21], [22], a sequential taguchi optimization method was improved. The high-dimensional

design would be optimized more quickly than conventional taguchi algorithms. While the accuracy of the algorithm was sacrificed, the efficiency was improved. The genetic algorithm technique was used to optimize the efficiency and torque of a permanent-magnet generator in which could arbitrarily select the number of optimization goals by non-dominated set ordering [23]. However, it increased the complexity and amount of calculation. For the complex structure of motor, most of optimization methods can not take into account the optimization accuracy, the solving speed and the search ability simultaneously. In this paper, the difficulty of motor optimization design is increased due to the special stator structure of DLW-HFTM. Therefore, the layered optimization of stator slot is built to reduce the difficulty of optimization and improve the optimization efficiency. The low and middle level parameters of DLW-HFTM are optimized by the response surface method because of the fast solving ability. It can establish multidimensional spatial surface through relatively few experimental arrays [24], [25]. However, it is not suitable to the high level parameters of DLW-HFTM because the accuracy of this method is not high. The quasi-newton method is to construct an objective function model to produce super-linear convergence by measuring the change of gradient. Reference [26] optimized an interior permanent magnetic BLDC motor through the quasi-newton method, it was found the quasi-newton method could improve solving speed and accuracy when the initial values of the iteration were close to the real solution values. Thus, the high level parameters of DLW-HFTM can be optimized to obtain higher accuracy through the quasi-newton method.

In this paper, the structure and winding connection of DLW-HFTM are introduced, and the finite model under the initial dimensions is established in Section II. In Section III, the design parameters are divided into three levels by multi-objective sensitivity analysis. Then, the parameters of different levels are respectively optimized with the torque, the torque ripple and the efficiency as the optimization objectives. In Section IV, the electromagnetic performance and fault-tolerant performance of DLW-HFTM are analyzed. The conclusion is given in Section V.

II. THE STRUCTURE OF DLW-HFTM
A. THE TOPOLOGY OF DLW-HFTM
Fig. 1 shows the 2D topology of three-phase, 10 pairs of poles DLW-HFTM, and each halbach array consists of five permanent magnets.

As shown in Fig. 2, the stator slot is divided into trapezoid-shaped upper slot and wine cup-shaped lower slot by slot wedge, and the upper and lower windings are arranged around the stator teeth, respectively. The stator slot is designed as arc-shaped opening slot, and the magnetic density of the stator teeth and the thermal load are decreased, thereby reducing the temperature of stator and solving the problem of local fever caused by excessive magnetic density in stator teeth [8].
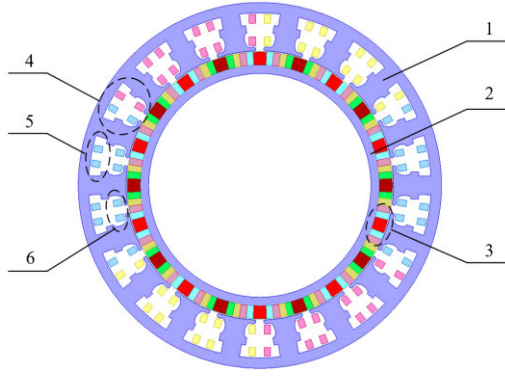
FIGURE 1. The 2D topology of DLW-HFTM. 1, stator; 2, rotor; 3, halbach arrays; 4, stator slot; 5, upper winding; 6, lower winding.
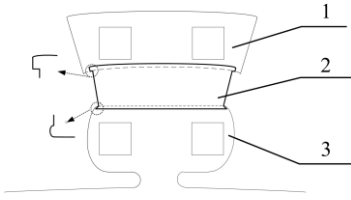

FIGURE 2. The structure of stator slot. 1, upper slot.

The slot wedge is designed as an I-shaped structure, and the enlarged view is shown in Fig. 2. It is facilitated to fix double-layer windings.

B. INITIAL DESIGN PARAMETERS OF DLW-HFTM
The output torque equation is shown in equation (1).

$$P_2 = \eta P_1 = \eta m E_m I_m \frac{\sqrt{2}\pi^3}{240} \frac{p}{P_s} k_d k_F k_{io}$$
$$(1 - k_{io}^2) A_c D_{so}^3 B_\delta C_s n\eta \quad (1)$$

where m is the number of phases, η is the efficiency of the motor, E_m is the magnitude of the induced electromotive force, I_m is the magnitude of the stator phase current, P_s is the number of stator slots, k_d is the winding factor, k_F is the air gap magnetic density distribution coefficient, k_{io} is split ratio, B_δ is the maximum value of the air-gap flux density, C_s is the calculating pole-arc coefficient, and A_c is the line load at the winding inner diameter, respectively.

Define the ratio of the inner diameter to the outer diameter of the stator as the split ratio of the motor, as shown in equation (2).

$$k_{io} = D_{si}/D_{so} \quad (2)$$

Equation (1) can be derived as equation (3).

$$D_{so}^3 = \frac{P_2}{\frac{\sqrt{2}p}{240P_s}\pi^3 k_d k_F k_{io}(1 - k_{io}^2)A_c B_\delta C_s n\eta} \quad (3)$$

According to equation (3), the initial parameter dimensions are obtained in order to design a DLW-HFTM with the rated power $P_N = 350$ W, the rated speed $n_N = 1500$ r/min, and

the rated voltage $U_N = 48$ V, as shown in TABLE 1. The geometric parameters of DLW-HFTM are shown in Fig. 3.
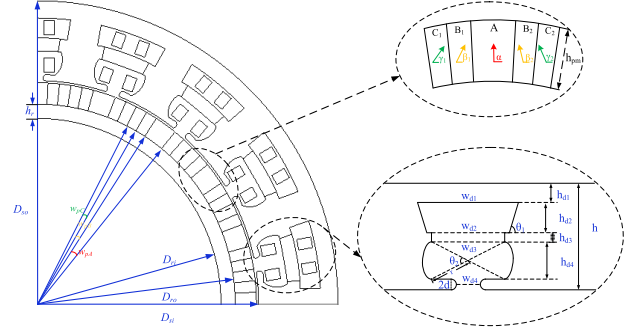

FIGURE 3. The parameter diagram of DLW-HFTM.

C. NORMAL WINDING CONNECTION OF DLW-HFTM
The stator winding coil distributions of 1/2 DLW-HFTM are shown in Fig. 4. The upper armature windings include A_{11}, A_{21}, A_{31} and so on, and the lower armature windings include A_{12}, A_{22}, A_{32} and so on.
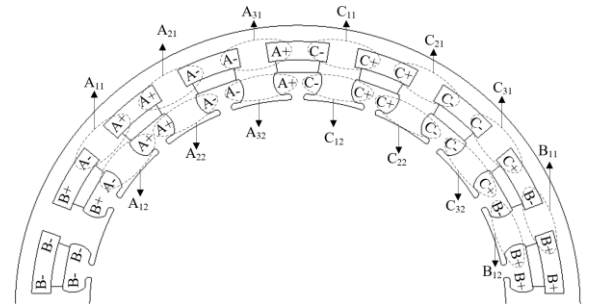

FIGURE 4. Distribution of stator winding coils in 1/2 DLW-HFTM.

The connection mode of winding can be divided into three cases as shown in Fig. 5.

The no-load back EMF waveforms of A phase are shown in Fig. 6. The amplitude of back EMF under the connection 1 is 26.02 V, which is increased by 3.5% and 1.1% than that under connection 2 and connection 3, respectively.

K_{Br} is the total harmonic distortion of air-gap flux density, which has a great influence on the output torque ripple.

$$K_{Br} = \sqrt{\sum_{i\neq 1}\left(\frac{B_{ri}}{B_r}\right)^2} \times 100\% \quad (4)$$

where B_{ri} is the *ith* harmonic amplitude of air-gap flux density, B_r is the fundamental component amplitude of air-gap flux density.

The air-gap magnetic density waveforms are compared in Fig. 7. By calculation, the K_{Br} of connection 1, connection 2 and connection 3 is 21.01%, 24.46% and 23.24%, respectively. The K_{Br} of connection 1 is reduced by 3.45% and 2.23% than that of connection 2 and connection 3, respectively.
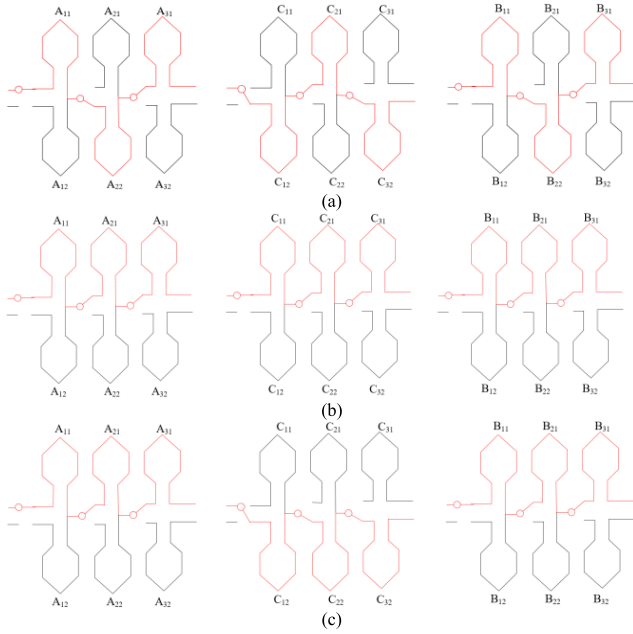
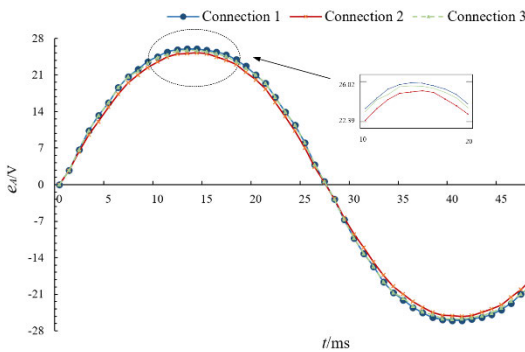**FIGURE 5.** Schematic diagram of winding connection. (a) Connection 1. (b) Connection 2. (c) Connection 3.

FIGURE 6. The no-load back EMF waveforms of A phase.

FIGURE 7. The waveform of air-gap magnetic density.
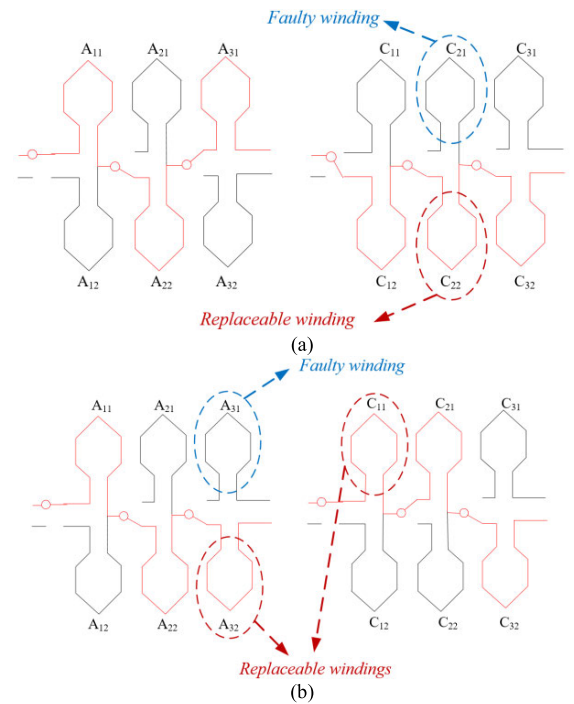
FIGURE 8. Schematic diagram of faulty winding connection. (a) Case1. (b) Case2.

Based on the above analysis, the connection 1 is selected as the winding connection mode of normal operation. In addition, this connection can also avoid short circuit fault between phases.

D. FAULTY WINDING CONNECTION OF DLW-HFTM

In order to improve the fault-tolerant performance of DLW-HFTM, the winding fault of the motor is analyzed as follows in Fig. 8.

When the C_{21} fails, it is replaced by the winding C_{22} of the same stator slot, but different layers, as shown in Fig. 8(a).

When the A_{31} fails, it is be replaced by A_{32} with the same stator slot, but different layers. Since the A_{32} and adjacent winding C_{12} are of different phases, the C_{12} is also replaced by the C_{11}, as shown in Fig. 8(b). In this way, the problem of short circuit between phase windings can be avoided. In order to simplify the description, fault 1 and fault 2 are used to represent the two different fault cases, respectively.
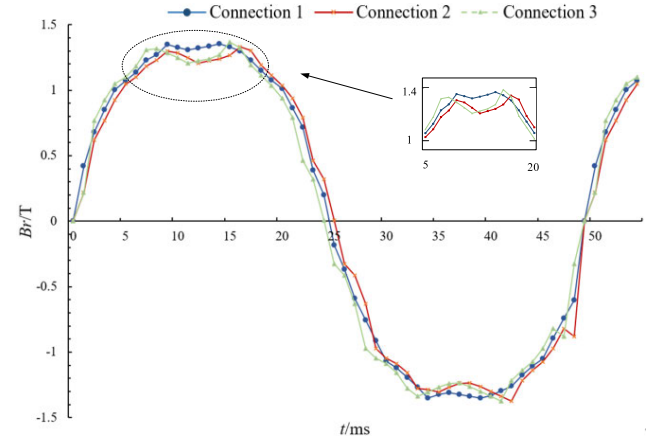
III. MUITI-OBJECTIVE LAYERED OPTIMIZATION

In order to achieve high efficiency η, large torque output T and lower torque ripple T_{ri}, the layered optimization of DLW-HFTM are carried out, and the flow chart is shown in Fig. 9.

The optimization model can be expressed as equation (5).

$$f(x_i) = \left\{ T(x_i)_{\max}, T_{ri}(x_i)_{\min}, \eta(x_i)_{\max} \right\} \quad (5)$$

Based on the practical requirements of joint robot motor, the multi-objective constraints are shown in equation (6).

$$\begin{cases} T \geq 1.2 T_N \\ T_{ri} \leq 5\% \\ \eta \geq 90\% \end{cases} \quad (6)$$

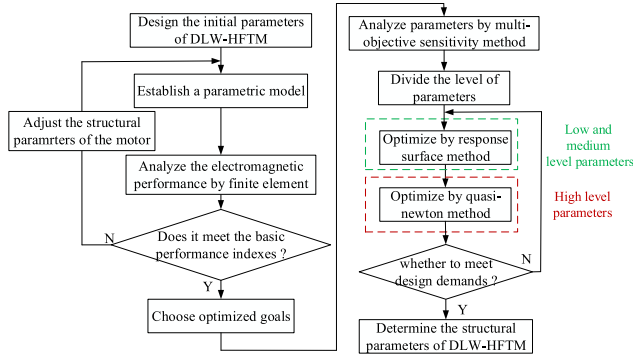where T_N is the rated torque, and the value is 2.2 Nm.

FIGURE 9. Schematic diagram of system flow.

A. SENSITIVE ANALYSIS

According to the method of [8], the main structural parameters are determined except the stator slot, as shown TABLE 1.

TABLE 1. The initial size of DLW-HFTM.

Parameter	Value	Parameter	Value
D_{si} (mm)	31.3	h_{d4} (mm)	4.6
D_{so} (mm)	42.5	d (mm)	0.52
D_{ri} (mm)	26	r (mm)	3.8
D_{ro} (mm)	28	W_{PA} (°)	6
h_{pm} (mm)	3	W_{PB} (°)	3
h_r (mm)	2	W_{PC} (°)	3
W_{d1} (mm)	9.6	α (°)	90
W_{d2} (mm)	8.6	β_1 (°)	30
W_{d3} (mm)	5	β_2 (°)	150
W_{d4} (mm)	1.8	γ_1 (°)	45
h_{d1} (mm)	2.4	γ_2 (°)	135
h_{d2} (mm)	3	θ_1 (°)	60
h_{d3} (mm)	0.8	θ_2 (°)	50

Because h is a fixed value, according to equations (7) - (9), the parameters of the stator slot affect each other. Therefore, the parameters shown in TABLE 2 are selected as the optimization variables of DLW-HFTM, and the value range are selected in TABLE 2.

$$h_{d1} = h - h_{d2} - h_{d3} - h_{d4} - d \quad (7)$$

$$h_{d4} = 2r \sin \frac{\theta_2}{2} \quad (8)$$

$$h_{d4} = \frac{w_{d3}}{2} \tan \frac{\theta_2}{2} \quad (9)$$

By equation (10), the parameter sensitivity of different structures $S(X)$ are calculation, and the radar diagram of multi-objective sensitivity analysis is shown in Fig. 10.

$$S(X) = Avg[S(Xi)] = Avg \left\{ \frac{\left\{ \frac{F(X0 \pm \Delta Xi) - F(X0)}{F(X0)} \right\}}{\left\{ \frac{\pm \Delta(Xi)}{X0} \right\}} \right\} \quad (10)$$

where X is the design parameter variable of DLW-HFTM, X_0 is the initial value of X, and X_i is defined as 10%, 15%, and 20% of its initial value, respectively. $S(X_i)$ is the parameter

sensitivity of the X_i. $Avg[S(X_i)]$ is the average value of the $S(X_i)$, and $F(X_0)$ is the value of optimizing the target under the condition of X_0.
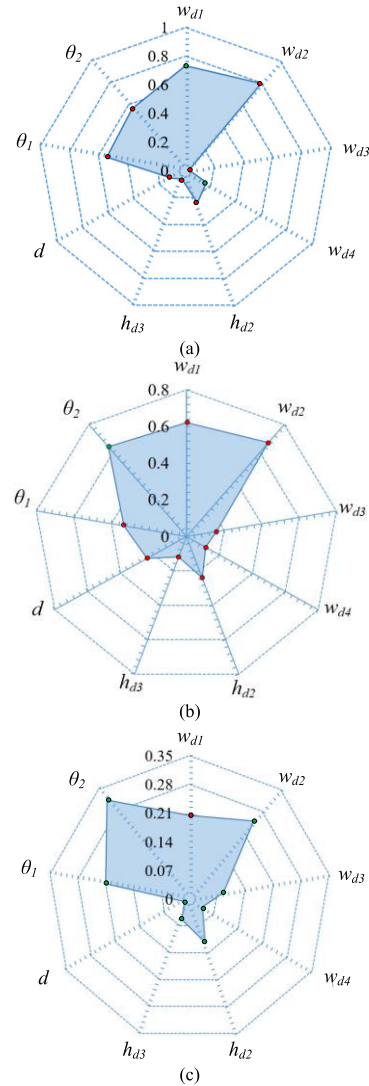

FIGURE 10. The radar diagram of multi-objective. (a) Output torque. (b) Torque ripple. (c) Efficiency.

The sensitivity analysis of the output torque, torque ripper and efficiency under the condition of the different design variables is shown in Fig. 10. If the sensitivity is far away from the center of the circle, the parameter variable is the more sensitive. Therefore, it is found from Fig. 10 that W_{d1} and W_{d2} are more sensitive to output torque, W_{d1}, W_{d2} and θ_2 are more sensitive to torque ripper, and θ_2 is more sensitive to efficiency.

In order to determine the impact of each parameter on the whole optimization goal, the comprehensive sensitivity equation S_c is shown in equation (11).

$$S_c(X) = \lambda_1 |S_T(X)| + \lambda_2 |S_{Tri}(X)| + \lambda_3 |S_\eta(X)| \quad (11)$$

where λ_i is the weight coefficient of the optimization goal. S_T is the sensitivity of the parameter to the torque, the S_{Tri} is the sensitivity of the parameter to the torque ripple, and the S_η is the sensitivity of the parameter to the efficiency.
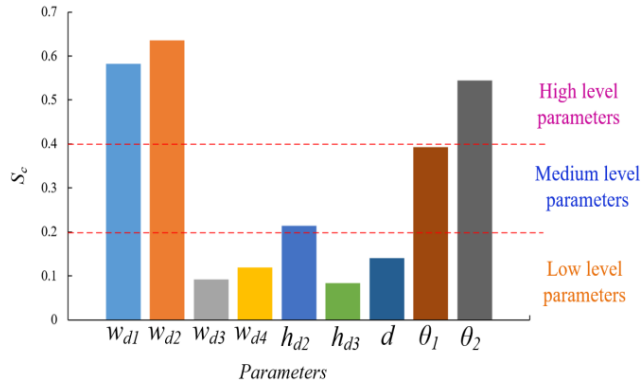

FIGURE 11. Schematic diagram of parameter level.

According to the importance of the optimization target in the application, the weight coefficient λ_1 and λ_2 in equation (12) are both selected as 0.4, and λ_3 is selected as 0.2. The sensitivity is divided into three levels, that is low level, medium level and high level, as shown in equation (12). It is seen from Fig. 11 that S_c of W_{d3}, W_{d4}, h_{d3} and d are less than 0.2, so they are low level parameters. Similarly, h_{d2} and θ_1 are middle level parameters because the S_c is between 0.2 and 0.4. W_{d1}, W_{d2} and θ_2 are high level parameters because the S_c is greater than 0.4.

$$Ranges \cong \begin{cases} Low\ level, & S_C \leq 0.2 \\ Medium\ level, & 0.2 \leq S_C \leq 0.4 \\ High\ level, & S_C \geq 0.4 \end{cases} \quad (12)$$

B. OPTIMIZATION OF LOW AND MEDIUM LEVEL PARAMETERS

According to the above analysis, the h_{d2}, h_{d3}, W_{d3}, W_{d4}, θ_1 and d are low and medium level parameters. Using the surface response method, these parameters are optimized to meet the optimization objectives. The relationships between each parameter and three optimization goals are shown in Fig. 12.

Fig. 12(a) shows that the torque T increases with the increase of h_{d2} and W_{d3}, and decreases first and then increases with the increase of W_{d4}, d and θ_1. In addition, it is found the value of T increases slowly with the increase of h_{d3}.

It can be seen from Fig. 12(b) that the torque ripple T_{ri} increases first and then decreases with the increase of h_{d2}, h_{d3}, θ_1 and d, and decreases first and then increases with the increase of W_{d4}, and the effect of W_{d3} on the T_{ri} is not obvious.

Fig. 12(c) displays the effect of parameters on efficiency. It can be found that the efficiency η increases slowly first and then decreases with the increase of W_{d4} and d. The value of the η increases slowly as the W_{d3} increases, and then rapidly

TABLE 2. Optimization range of parameters.

Parameter	Value range
W_{d1} (mm)	7.68~11.52
W_{d2} (mm)	6.88~10.32
W_{d3} (mm)	4.5~7.5
W_{d4} (mm)	1.4~2.2
h_{d2} (mm)	2.4~3.8
h_{d3} (mm)	0.55~0.85
d (mm)	0.4~0.625
θ_1 (º)	4.5~7.5
θ_2 (º)	59.2~88.8

decreases. But the effect of θ_1 on η is the opposite with W_{d3}. It is found that the value of the h_{d3} is proportional to the value of the η. Combined with the above analysis, the parameter values of W_{d3}, W_{d4}, h_{d2}, h_{d3}, d and θ_1 are designed as 6mm, 1.7 mm, 2.8 mm, 0.7 mm, 0.5 mm, and 65º, respectively.

C. OPTIMIZATION OF HIGH LEVEL PARAMETERS

On the basis of the above optimal dimensions, the output torque of DLW-HFTM is 2.43 Nm, the torque ripple is 6.07%, and the efficiency is 83.7%, which are close to the optimization objectives in equation (6). Therefore, the quasi-newton method can be used to optimize high level parameters W_{d1}, W_{d2} and θ_2. Its iterative formula is in equation (13).

$$X_{k+1} = X_k - \alpha_k B_k^{-1} \nabla f(X_k) \quad (13)$$

where α_k is a linear search step factor, and the B_k is a symmetric positive definite matrix.

The quasi-newtonian condition is shown in equation (14).

$$B_{k+1} s_k = y_k \quad (14)$$

where $s_k = X_{k+1} - X_k$, $y_k = \nabla f(X_{k+1}) - \nabla f(X_k)$.

The stator slot structure parameters of DLW-HFTM are determined on basis of the above analysis and are shown in TABLE 3.

TABLE 3. The parameters of stator slot.

Performance	Initial value	Optimal value
W_{d1}/ mm	9.6	9.6
W_{d2}/ mm	8.6	7.74
W_{d3}/ mm	5	6
W_{d4}/ mm	1.8	1.7
h_{d2}/ mm	3	2.8
h_{d3}/ mm	0.8	0.7
d/ mm	0.52	0.5
θ_1/ º	60	65
θ_2/ º	50	43.5

IV. ANALYSIS OF OPTIMAL RESULTS
A. COMPARISON OF ELECTROMAGNETIC PERFORMANCE
Fig. 13 show the magnetic induction line of 1/2 DLW-HFTM, and it is found that the larger output torque can be provided
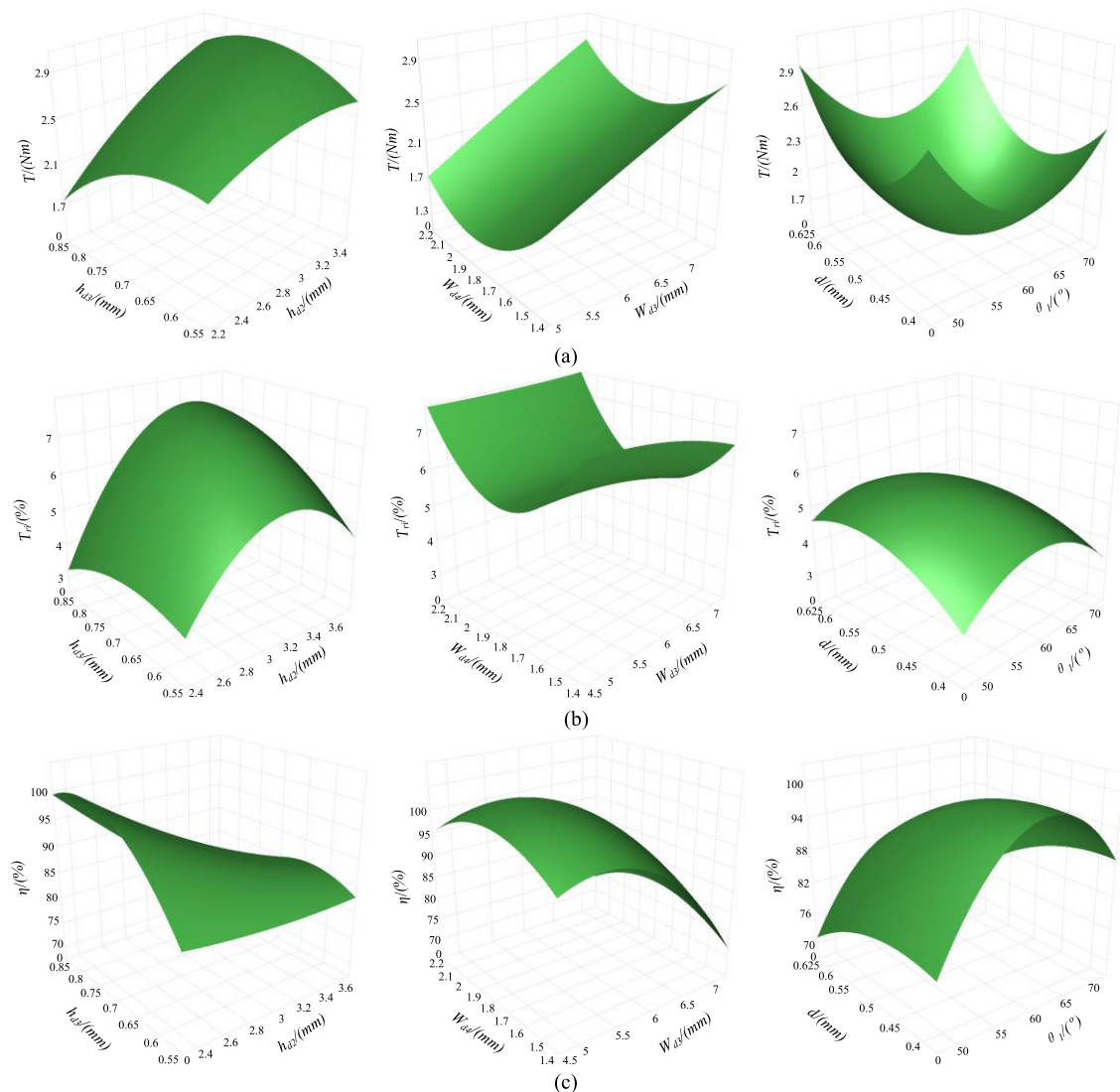
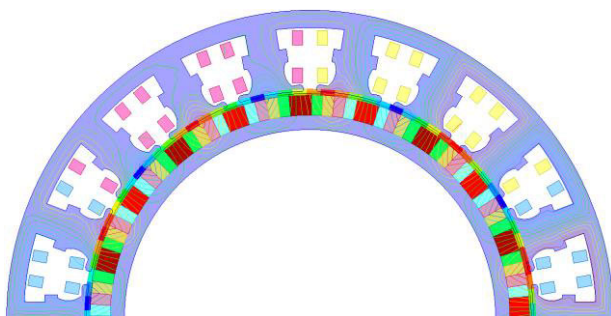**FIGURE 12.** Surface response with different parameters.(a) Output torque. (b) Torque ripple. (c) Efficiency.

FIGURE 13. The magnetic induction line of 1/2 DLW-HFTM.

FIGURE 14. The waveform of output torque.

due to the excellent single-side magnetization effect of the halbach arrays.

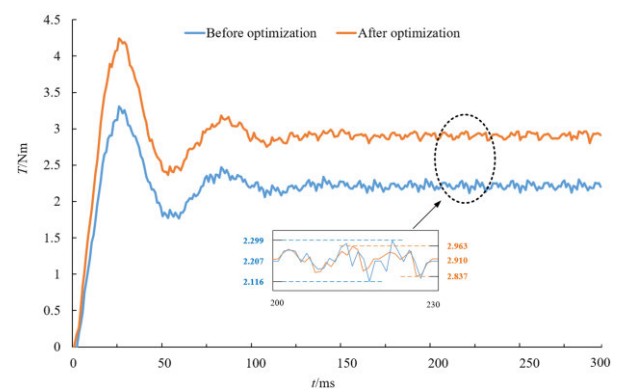The maximum output torque waveforms at rated speed 1500 r/min before and after DLW-HFTM are compared and shown in Fig. 14. The output torque after optimization is 2.91 Nm, which is 31.85% higher than that before optimization, and 1.31 times of T_N. The torque ripple is 3.96%, which is lower than that before optimization.

TABLE 4. The loss and efficiency of DLW-HFTM.

Performance	Before optimization	After optimization
P_{Cu} (W)	30.69	27.51
P_{Fe} (W)	9.43	9.48
η (%)	90.9	92.2

TABLE 4 shows the loss and efficiency of before and after DLW-HFTM optimization under the rated condition. The iron loss and the copper loss of DLW-HFTM are indicated by P_{Fe} and P_{Cu}, respectively.

After optimization, the iron loss of DLW-HFTM is 9.48 W which is similar to before optimization. However, the copper loss of DLW-HFTM after optimization is reduced by 3.18 W than that before optimization. The total loss of the optimized motor is reduced, and the efficiency of the motor is increased to 92.2%, which meets the design requirement.
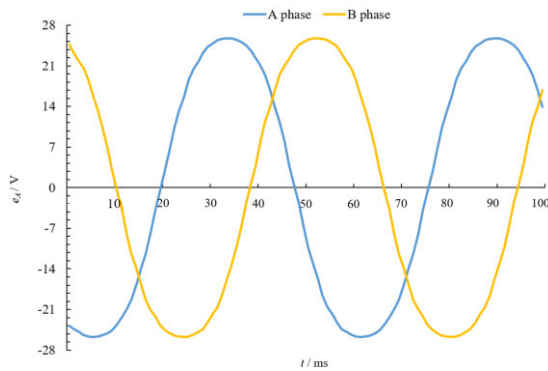

FIGURE 15. The three-phase no-load back EMF waveform of fault 1.

B. ANALYSIS OF FAULT-TOLERANT PERFORMANCE

The three-phase no-load back EMF under fault 1 described in Fig. 8(a) are shown in Fig. 15, at the rated speed 1500 r/min. The C phase is lost due to C_{21} open-circuit fail.

TABLE 5. The performance of before and after failt-tolerant.

Performance	Before fault-tolerant	After fault-tolerant	
		Case 1	Case 2
e_A (V)	26.02	25.73	25.79
T (Nm)	2.91	2.84	2.82
T_{ri} (%)	3.96	6.33	5.67
P_{Cu} (W)	27.51	35.94	38.29
P_{Fe} (W)	9.48	9.23	9.31
η (%)	92.2	87.1	86.4

The fault-tolerant performances of case 1 are shown in Fig.16. The three-phase no-load back EMF are shown in Fig. 16(a). The winding C_{21} is replaced by the winding C_{22}, and the amplitude of the no-load back EMF is 25.73 V, which
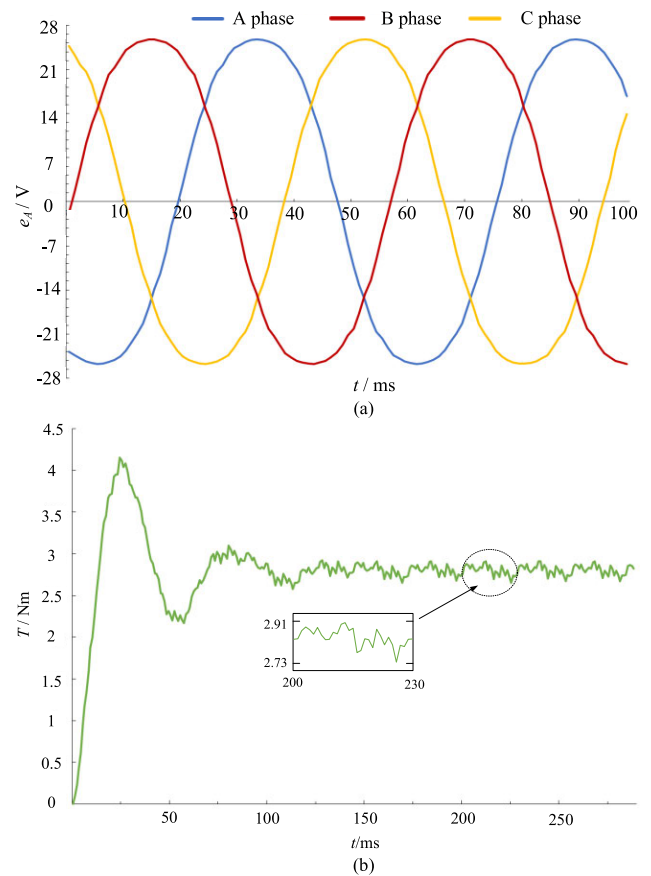

FIGURE 16. The fault tolerant performance under the case 1. (a) Three-phase no-load back EMF waveform. (b) Output torque waveform.
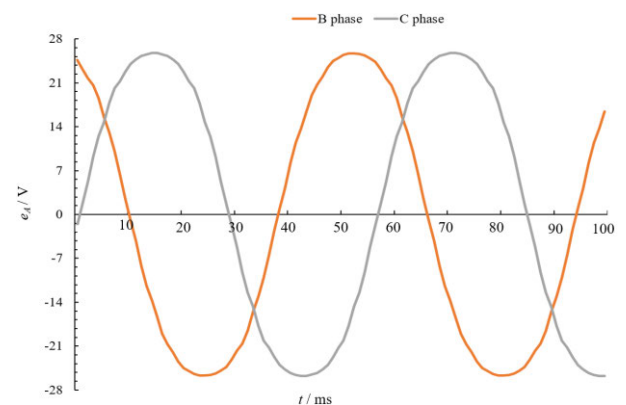

FIGURE 17. The three-phase no-load back EMF waveform of fault 2.

is 0.29 V lower than that of the normal operation in Fig. 6, the error is less than 2%. The output torque waveform is show in Fig. 16(b), at the rated speed 1500 r/min. The torque is 2.84 Nm, and torque ripple is 6.33%. In fault tolerant case 1, the torque is reduced by 2.4% in contrast with the normal operation, the torque ripple is increased by 2.37%, and the efficiency is reduced to 87.1%, as shown in TABLE 5.
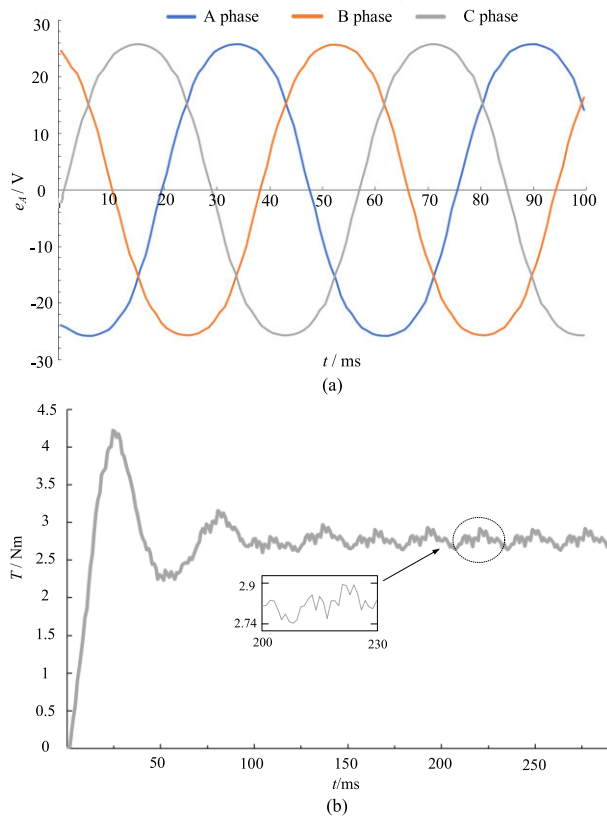
FIGURE 18. The performances of case 2. (a) Three-phase no-load back EMF waveform. (b) Output torque waveform.

Similarly, three-phase no-load back EMF of fault 2 described in Fig. 8(b) is shown in Fig. 16.

When the fault 2 happens, the fault-tolerant performance of case 2 is shown in Fig. 18 and TABLE 5. Fig. 18(a) indicates that the back EMF amplitude is 25.79 V, less than 2% than the normal operation. Fig. 18(b) is the output torque waveform under fault tolerant case 2, at the rated speed 1500 r/min. The torque is 2.82 Nm, and the torque ripple is 5.67%, and the efficiency is 86.4%.

V. CONCLUSION

A new type of joint motor for robot is proposed in this paper. A hierarchical optimization method based on parameter sensitivity analysis is used to determine the optimal structural parameters of the motor quickly and effectively. The parameters of medium and low level are optimized by response surface method, the high level parameters vel are optimized by quasi-newton method. Compared with the design requirements of DLW-HFTM, the torque is increased by 31.85%, the torque ripple is reduced by 3.96%, and the efficiency is increased by 2.2% through the optimal method. When the open-circuit fault happens under the rated condition, switching the winding connection can satisfy the demand of torque. Although the efficiency is lightly reduced and the torque ripple is lightly increased, it is noted the DLW-HFTM can improve the fault-tolerance without the complex control algorithms.

REFERENCES

[1] S. Hussain, P. K. Jamwal, P. Van Vliet, and M. H. Ghayesh, "State-of-the-art robotic devices for wrist rehabilitation: Design and control aspects," *IEEE Trans. Human-Machine Syst.*, vol. 50, no. 5, pp. 361–372, Oct. 2020.

[2] Y. Li, X. Guan, Z. Li, Z. Tang, B. Penzlin, Z. Yang, S. Leonhardt, and L. Ji, "Analysis, design, and preliminary evaluation of a parallel elastic actuator for power-efficient walking assistance," *IEEE Access*, vol. 8, pp. 88060–88075, 2020.

[3] J. Lee, H. Yeo, H. Jung, T. Kim, and J. Ro, "Electromagnetic and thermal analysis and design of a novel-structured surface-mounted permanent magnet motor with high-power-density," *IET Electr. Power Appl.*, vol. 13, no. 4, pp. 472–478, Apr. 2019.

[4] Y. Ayalon, L. Damti, and D. Zarrouk, "Design and modelling of a minimally actuated serial robot," *IEEE Robot. Autom. Lett.*, vol. 5, no. 3, pp. 4899–4906, Jul. 2020.

[5] A. De, A. Stewart-Height, and D. E. Koditschek, "Task-based control and design of a BLDC actuator for robotics," *IEEE Robot. Autom. Lett.*, vol. 4, no. 3, pp. 2393–2400, Jul. 2019.

[6] C. L. C. Bual, R. D. Cunanan, R. A. R. Bedruz, A. A. Bandala, R. R. P. Vicerra, and E. P. Dadios, "Design of controller and PWM-enabled DC motor simulation using proteus 8 for flipper track robot," in *Proc. IEEE 11th Int. Conf. Humanoid, Nanotechnol., Inf. Technol., Commun. Control, Environ., Manage. (HNICEM)*, Laoag, Philippines, Nov. 2019, pp. 1–5.

[7] X. Liu, H. Chen, J. Zhao, and A. Belahcen, "Research on the performances and parameters of interior PMSM used for electric vehicles," *IEEE Trans. Ind. Electron.*, vol. 63, no. 6, pp. 3533–3545, Jun. 2016.

[8] S. Zhang, W. Zhang, R. Wang, X. Zhang, and X. Zhang, "Optimization design of Halbach permanent magnet motor based on multi-objective sensitivity," *CES Trans. Electr. Mach. Syst.*, vol. 4, no. 1, pp. 20–26, Mar. 2020.

[9] P. T. Luu, J.-Y. Lee, J.-H. Lee, and J.-W. Park, "Electromagnetic and thermal analysis of permanent-magnet synchronous motors for cooperative robot applications," *IEEE Trans. Magn.*, vol. 56, no. 3, pp. 1–4, Mar. 2020.

[10] H. Tang, M. Zhang, Y. Dong, W. Li, and L. Li, "Influence of the opening width of stator semi-closed slot and the dimension of the closed slot on the magnetic field distribution and temperature field of the permanent magnet synchronous motor," *IET Electr. Power Appl.*, vol. 14, no. 9, pp. 1642–1652, Sep. 2020.

[11] Y. Demir and M. Aydin, "A novel dual three-phase permanent magnet synchronous motor with asymmetric stator winding," *IEEE Trans. Magn.*, vol. 52, no. 7, pp. 1–5, Jul. 2016.

[12] Q. Chen, Y. Yan, G. Liu, and G. Xu, "Design of a new fault-tolerant permanent magnet machine with optimized salient ratio and reluctance torque ratio," *IEEE Trans. Ind. Electron.*, vol. 67, no. 7, pp. 6043–6054, Jul. 2020.

[13] M.-A. Shamsi-Nejad, B. Nahid-Mobarakeh, S. Pierfederici, and F. Meibody-Tabar, "Fault tolerant and minimum loss control of double-star synchronous machines under open phase conditions," *IEEE Trans. Ind. Electron.*, vol. 55, no. 5, pp. 1956–1965, May 2008.

[14] Y. Zhao and T. A. Lipo, "Modeling and control of a multi-phase induction machine with structural unbalance," *IEEE Trans. Energy Convers.*, vol. 11, no. 3, pp. 570–577, Sep. 1996.

[15] F.-J. Lin, I.-F. Sun, K.-J. Yang, and J.-K. Chang, "Recurrent fuzzy neural cerebellar model articulation network fault-tolerant control of six-phase permanent magnet synchronous motor position servo drive," *IEEE Trans. Fuzzy Syst.*, vol. 24, no. 1, pp. 153–167, Feb. 2016.

[16] S. Ahmed, C. Grabher, H.-J. Kim, and T. Koseki, "Multifidelity surrogate assisted rapid design of transverse-flux permanent magnet linear synchronous motor," *IEEE Trans. Ind. Electron.*, vol. 67, no. 9, pp. 7280–7289, Sep. 2020.

[17] Y. Hua, H. Zhu, and Y. Xu, "Multi-objective optimization design of bearingless permanent magnet synchronous generator," *IEEE Trans. Appl. Supercond.*, vol. 30, no. 4, pp. 1–5, Jun. 2020.

[18] Z. Ji, H. Zhu, Y. Xu, and M. Wu, "Optimization design of permanent magnet assisted single winding bearingless synchronous reluctance motor," *IEEE Trans. Appl. Supercond.*, vol. 30, no. 4, pp. 1–5, Jun. 2020.

[19] J. Li, X. Huang, B. Zhou, H. Yu, and Q. Huang, "Design principle of a 16-pole 18-slot two-sectional modular permanent magnet linear synchronous motor with optimisation of its end tooth," *IET Electr. Power Appl.*, vol. 14, no. 3, pp. 441–447, Mar. 2020.

[20] Y. Li, C. Zhu, L. Wu, and Y. Zheng, "Multi-objective optimal design of high-speed surface-mounted permanent magnet synchronous motor for magnetically levitated flywheel energy storage system," *IEEE Trans. Magn.*, vol. 55, no. 7, pp. 1–8, Jul. 2019.

[21] Z. Shi, X. Sun, G. Lei, Z. Yang, Y. Guo, and J. Zhu, "Analysis and optimization of radial force of permanent-magnet synchronous hub motors," *IEEE Trans. Magn.*, vol. 56, no. 2, pp. 1–4, Feb. 2020.

[22] J. Cui, W. Xiao, W. Zou, S. Liu, and Q. Liu, "Design optimisation of submersible permanent magnet synchronous motor by combined DOE and taguchi approach," *IET Electr. Power Appl.*, vol. 14, no. 6, pp. 1060–1066, Jun. 2020.

[23] J. Xu, B. Zhang, X. Kuang, H. Guo, and S. Guo, "Influence analysis of slot parameters and high torque density optimisation for dual redundant permanent magnet motor in aerospace application," *IET Electr. Power Appl.*, vol. 14, no. 7, pp. 1263–1273, Jul. 2020.

[24] G. Liu, Y. Wang, Q. Chen, G. Xu, and C. Song, "Multiobjective deterministic and robust optimization design of a new spoke-type permanent magnet machine for the improvement of torque performance," *IEEE Trans. Ind. Electron.*, vol. 67, no. 12, pp. 10202–10212, Dec. 2020.

[25] J. He, G. Li, R. Zhou, and Q. Wang, "Optimization of permanent-magnet spherical motor based on taguchi method," *IEEE Trans. Magn.*, vol. 56, no. 2, pp. 1–7, Feb. 2020.

[26] M. Khelifa, M. Mordjaoui, and A. Medoued, "An inverse problem methodology for design and optimization of an interior permanent magnetic BLDC motor," *Int. J. Hydrogen Energy*, vol. 42, no. 28, pp. 17733–17740, Jul. 2017.
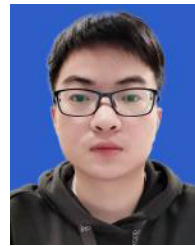
WEI ZHANG (Member, IEEE) was born in Taizhou, Jiangsu, China, in 1977. She received the B.Sc. degree in electrical engineering from Nantong University, Nantong, China, in 2000, and the M.Sc. and Ph.D. degrees in electrical engineering from Southeast University, Nanjing, China, in 2007 and 2016, respectively. From January 2017 to December 2017, she was a Visiting Scholar with The University of Sheffield, Sheffield, U.K. Since 2000, she has been with the College of Electrical Engineering, Nantong University, as a Professor.

Her current major research interests include design and control of permanent magnet brushless machines and drives for automotive applications, and renewable energy applications.

JIANWEI ZHAO was born in Bozhou, Anhui, China, in 1996. He received the B.Sc. degree in electrical engineering and automation from the Anhui University of Science and Technology, Bengbu, China, in 2020. He is currently pursuing the M.Sc. degree in control science and engineering with Nantong University, Nantong, China.

His current research interest includes design and optimization of motors.

SHUANGSHUANG ZHANG was born in Yancheng, Jiangsu, China, in 1995. She received the B.Sc. degree in electrical engineering from the Zhonghuan Information College, Tianjin University of Technology, Tianjin, China, in 2018. She is currently pursuing the M.Sc. degree in control science and engineering with Nantong University, Nantong, China.

Her current research interest includes design and optimization of halbach motors.

RUI WANG was born in Huaian, Jiangsu, China, in 1997. He received the B.Sc. degree in electrical engineering and intelligent control from Nantong University, Nantong, China, in 2019, where he is currently pursuing the M.Sc. degree in control science and engineering.

His current research interest includes design and optimization of axial field flux-switching permanent magnet machine.

• • •